Journal of Food and Drug Analysis

Volume 30
Issue 4 *Special Issue*

Article 8

Optimum synthesis of Au@Ag nanoparticle as plasma amplifier to detect trace concentration of AFB1 via object-binder-metal SERS method

Recommended Citation

Chen, Wenwen; Chen, Qiang; Zhang, Wei; Zhang, De; Yu, Zhi; Song, Ying; Zhang, Xiubing; Ni, Dejiang; and Liang, Pei (2022) "Optimum synthesis of Au@Ag nanoparticle as plasma amplifier to detect trace concentration of AFB1 via object-binder-metal SERS method," *Journal of Food and Drug Analysis*: Vol. 30 : Iss. 4 , Article 8.
Available at: https://doi.org/10.38212/2224-6614.3418

Optimum synthesis of Au@Ag nanoparticle as plasma amplifier to detect trace concentration of AFB1 via object-binder-metal SERS method

Cover Page Footnote

The work was financially supported by the National Key Research and Development Program of China (Grant No.2021YFD1000401), and the Hubei Provincial Water Resources Key Research Project (Grant No. HBSLKJT202001).

Optimum synthesis of Au@Ag nanoparticle as plasma amplifier to detect trace concentration of AFB1 via object-binder-metal SERS method

Wenwen Chen [a,b,1], Qiang Chen [c,1], Wei Zhang [a], De Zhang [a,b], Zhi Yu [b,*], Ying Song [b], Xiubing Zhang [a], Dejiang Ni [b], Pei Liang [a,**]

[a] College of Optical and Electronic Technology, China Jiliang University, 310018, Hangzhou, China
[b] College of Horticulture & Forestry Sciences, Huazhong Agricultural University, Key Laboratory of Horticultural Plant Biology, Ministry of Education, 430070, Wuhan, China
[c] College of Metrology and Measurement Engineering, China Jiliang University, 310018, Hangzhou, China

Abstract

The problem of aflatoxin contamination emerged gradually in the field of food safety. Surface-enhanced Raman spectroscopy (SERS) is an ultra-sensitive and non-destructive spectroscopy technology with extensive application prospects in the detection field. In this paper, with the detection of AFB1 as the target, Au@Ag NPs substrate with uniform morphology and strong SERS effect was prepared. Furthermore, the intermediates formed by hydrogen bonding between AFB1 and melamine facilitate the binding of toxin molecules to the substrate. Moreover, the AFB1-melamine-Au@Ag NPs detection system was established by optimizing the melamine dosage, and the limit of detection can reach 10^{-8} mol/L (M). In this method, AFB1 (concentration range of 10^{-4} M -10^{-7} M) in tea oil, the Raman signal intensity of AFB1 shows an excellent linear, logarithmic relationship, and the correlation coefficient is 0.9685. Therefore, this work has achieved simple, sensitive, and stable AFB1 detection and has broad application potential in food safety detection.

Keywords: AFB1, Au@Ag NPs, Melamine, SERS

1. Introduction

In food safety, aflatoxin pollution is more prominent, especially in foods such as oil, peanuts, and wheat [1,2]. Aflatoxin B1 (AFB1) has potent carcinogenicity, mutagenicity, teratogenicity, and organ toxicity [3,4]. At present, the detection methods of AFB1 mainly focus on high-performance liquid chromatography (HPLC), enzyme-linked immunosorption (ELISA), thin layer analysis (TLC), and capillary electrophoresis (CE) [5,6]. However, the above methods have many problems, such as complicated pretreatment, toxic reagent, expensive instrument, low detection sensitivity, and false-positive results [7,8]. Therefore, it is significant to develop a fast and effective analytical method to detect AFB1.

SERS technology has the advantages of convenient operation, high sensitivity, quickness to respond, low cost, simplicity, and extensive application advantages in fungal toxin detection [9–11]. However, the strength of the SERS effect has a great relationship with the substrate structure, shape, size, and the combination mode of the measured material [12,13]. Whether molecules were adsorbed on the surface of the substrate and the morphology of molecules adsorbed on the surface of the substrate are the main factors of the signal strength of SERS enhanced effect [14,15]. So far, it is a research hotspot to increase the types of SERS substrate

Received 21 January 2022; accepted 6 June 2022.
Available online 23 November 2022

* Corresponding author.
** Corresponding author.
E-mail addresses: yuzhipl@163.com (Z. Yu), Plianghust@gmail.com (P. Liang).
[1] The authors contributed equally to this paper.

https://doi.org/10.38212/2224-6614.3418

materials, enhance signals' stability, and improve detection sensitivity and accuracy to obtain a lower detection limit [16,17].

Au, Ag, and other noble metal materials are often used as SERS substrates to achieve a better SERS enhancement effect. Their local plasma resonance absorption peak can cover the common Raman laser light source, combining with the molecules to be measured effectively [18,19]. To date, sensitivity, stability, and repeatability can be further optimized in the study of SERS substrate [20,21]. Furthermore, Ag nanoparticles have strong SERS enhancement ability, and Au nanoparticles have good biological compatibility and stability [22,23]. Therefore, combined with the respective advantages of Au and Ag, the Au@Ag composite substrate has become a research hotspot [24].

Using noble metal nanoparticles as SERS substrate to detect AFB1 can be roughly divided into two categories. The first category is to realize SERS detection by relying on the direct action of AFB1 and substrate. The second category is modifying the substrate. First, the target molecules are close to the SERS substrate surface with the help of physical or chemical adsorption, then to realize SERS detection. Qu et al. developed a method to detect aflatoxin (AFs) in situ using thin layer chromatography combined with surface-enhanced Raman spectroscopy (TLC-SERS). This method was simple to operate, but the detection limit of AFB1 could only reach 10^{-6} M [25]. Many researchers use aptamer and antibody to detect AFB1, reaching the detection limit of lower concentration [26]. AFB1 performed SERS detection directly with low sensitivity in the above detection, but the detection process through antigen–antibody, aptamer, and other methods was complex. Studies have shown that the substance to be measured can form a close combination with the substrate utilizing intermediates to achieve simple and effective SERS enhancement [27–30]. An et al. showed that the combination of SERS and DFT provided key in situ molecular entities, revealing the presence of surface intermediates under the strong electrocatalytic performance of silver electrodes [31]. The force between the intermediate and the object is measured to promote the SERS effect. The adsorption energy is calculated using DFT so that SERS detection can be carried out effectively. However, the practical application of this method in AFB1 and metal nanoparticles needs further research.

Based on the previous studies on gold and silver nanoparticles, this study selected Ag NPs and Au NPs with a strong Raman enhancement effect as the basis to further prepare Au@Ag composite substrate. Furthermore, melamine can be adsorbed onto nanoparticles and form hydrogen bonds with AFB1. Therefore, the SERS detection system of AFB1-melamine-Au@Ag NPs is established to detect AFB1.

2. Materials and methods

2.1. Materials and reagents

Chlorauric acid($HAuCl_4$), sodium citrate ($Na_3C_6H_5O_7$), phloroccinol($C_6H_6O_2$), silver nitrate ($AgNO_3$), ascorbic acid(ASA), polyvinylpyrrolidone (PVP), sodium hydroxide(NaOH), crystal violet(CV), aflatoxin B1(AFB1), melamine, tricyanic acid and p-amino thiophenol (4-ATP) were all purchased from Aladdin Reagent Co., LTD. (Shanghai, China). Tea oil Sample 1 (brand: Qian Daoyuan, origin: Zhejiang Province, China). Tea oil Sample 2 (brand: Qian Suihao, origin: Jiangxi Province, China). Tea oil Sample 3 (brand: Dong Cha, origin: Zhejiang Province, China). Without further purification, anhydrous ethanol was purchased from Zhejiang Sanying Chemical Reagent Co., LTD. (Zhejiang, China). All aqueous solution was prepared with deionized water and Millipore Milli - Q system purification (18.2 MΩ/cm, Bedford, MA, USA).

2.2. Preparation of nanoparticles as SERS substrate

In this paper, we refer to the previous research on the preparation of nanoparticles by our research group and further synthesize alloy nanoparticles based on flower-like silver nanoparticles and gold nanoparticles [32–35]. The specific steps are as follows:

2.2.1. Ag nanoparticles

10 mL deionized water, 200 μL $AgNO_3$ (1M), and 2 mL PVP (1%wt) were added to the beaker and placed on a magnetic agitator. After stirring for 2 min, 1 mL ASA (0.1M) was added, and Ag nanoparticles (Ag NPs) were obtained after stirring for 10 min.

2.2.2. Au nanostars

First, the beaker was placed on the magnetic heating agitator and was added 30 mL of deionized water to heat and boil; then was added 300 μL $HAuCl_4$ (0.024 M) to boil and stirred for 2 min 900 μL $Na_3C_6H_5O_7$ (1% wt) was added to the beaker to heat and boil until the solution became wine-red and golden seeds were formed. Subsequently, the beaker was placed on a magnetic heating agitator, then 10 mL deionized water, 400 μL $HAuCl_4$(0.1 M), 50 μL of the above formed gold seeds, 200 μL

$Na_3C_6H_5O_7$ (1%wt) and 1 mL $C_6H_6O_2$(0.05 M) was added. Au nanostars (Au NSs) were obtained after stirring at 50 °C for 30 min.

2.2.3. Au@Ag nanostars

6 mL PVP (1%wt) was added to the beaker. Then 10 mL Au NSs solution prepared in 2.2.1 was added to the above solution and was stirred with a magnetic agitator. Then, 0.4 mL ASA (0.1 M), 0.5 mL $AgNO_3$(0.01 M) and 0.8 mL NaOH (0.1 M) were added. After stirring for 5 min, the solution turned wine red, and Au@Ag nanostars (Au@Ag NSs) were obtained.

2.2.4. Ag@Au nanoparticles

100 mg ASA and 66.6 mg PVP were dissolved in 15 mL deionized water under magnetic stirring. Then, 5 mL Ag NPs prepared in 2.2.2. were added to the above solution. Then 1 mL NaOH (0.1M) and 700 μL $HAuCl_4$ (0.1 M) (10 μL/min) were added in sequence. The color of the solution changed from dark blue to pink, indicating the formation of Ag@Au nanoparticles (Ag@Au NPs).

2.2.5. Au@Ag nanoparticles

First, 3 mL gold seeds are prepared in 2.2.1. and 400 μL ASA (0.1 M) were added to the beaker under magnetic stirring. Then, 0.9 mL $AgNO_3$ (0.001 M) (10 μL/min) was added by dropping to prepare Au@Ag nanoparticles (Au@Ag NPs). During this process, the solution color changed from burgundy to orange, indicating a silver layer grown on the outer layer of the gold core.

Then, according to the above different nanoparticles, deionized water was used five times of repeated centrifugation at a speed of 10,000 r/min to remove impurities on the surface of nanoparticles and colloidal particles with different morphology dispersed in 10 mL ultrapure water were obtained. After that, 30 μL of gold colloidal particles were sucked into a customized glass tank (diameter: 5 mm; Depth: 3 mm) by a pipette and were dried in a vacuum drying oven. Finally, different concentrations of the solution to be measured were titrated onto the substrate to be used for Raman detection.

2.3. Nanoparticle characterizations and SERS measurements

2.3.1. Preparation of the test substance

CVs with different concentrations are directly dropped on the substrate for CV detection. In detecting pure AFB1, different concentrations of AFB1 and intermediates were mixed, respectively, and the mixture was dropped on the substrate for detection. When detecting aflatoxin B1 in tea oil, mix AFB1, tea oil, and melamine with different concentrations, and drop the mixture on the substrate for detection. The above mixing methods are: mixing on a magnetic stirrer for 5 min.

2.3.2. Test equipment and conditions

A scanning electron microscope (HITACHI, SU8010 FE-SEM) was used for size and morphology analysis, and transmission electron microscope (TEM) analysis was performed using JEM-1400Plus (120 kV, HITACHI). UV–Vis absorption spectrum was reported at 400–800 nm on a UV–Vis spectrophotometer (TU-1901, Purkinye, China). The electromagnetic field of nanoparticles was simulated using 3D-FDTD software to obtain the electromagnetic enhancement effect of nanoparticles (Lumerical FDTD Solutions 8.19.1584). Surface-enhanced Raman scattering (SERS) spectra of all samples were collected and recorded on the confocal Raman microscope system (LabRAM HR, Horiba) and a portable Raman instrument. The excitation wavelength was 532/633/785 nm, and the laser diameter was 5 mm, irradiating vertically on the test substrate. The detection conditions of CV and pure AFB1 are: each scan time is 10 s, laser power is 2.5%, and recorded on LabRAM HR. The detection conditions of AFB1 in Tea oil are: each scan time is 5s, the laser power is 50 mW, and it is recorded on a portable Raman instrument. All measurements are randomly performed 3 times on the surface of the substrate.

3. Results and discussions

The experimental flow chart is shown in Fig. 1. Firstly, nanoparticles were prepared in five different ways, and the morphology and size of nanoparticles were analyzed. Secondly, the nanoparticles were applied to SERS detection of CV, and the advantages and disadvantages of their SERS enhanced effect were compared to optimize the best substrate. Finally, the optimal nanoparticle substrate was applied to the detection of AFB1. Notably, the direct test effect after mixing nanoparticles and AFB1 is not good in detecting AFB1 because of the weak adsorption of nanoparticles and AFB1. In addition, melamine and AFB1 formed hydrogen bond forces to promote the SERS effect. Therefore, the SERS detection system of AFB1-melamine-NPs was established to realize the effective detection of AFB1.

3.1. Optimization of nanoparticles under different growth conditions

In this paper, Ag NPs, Au NSs, Au@Ag NSs, Ag@Au NPs, and Au@Ag NPs were prepared using

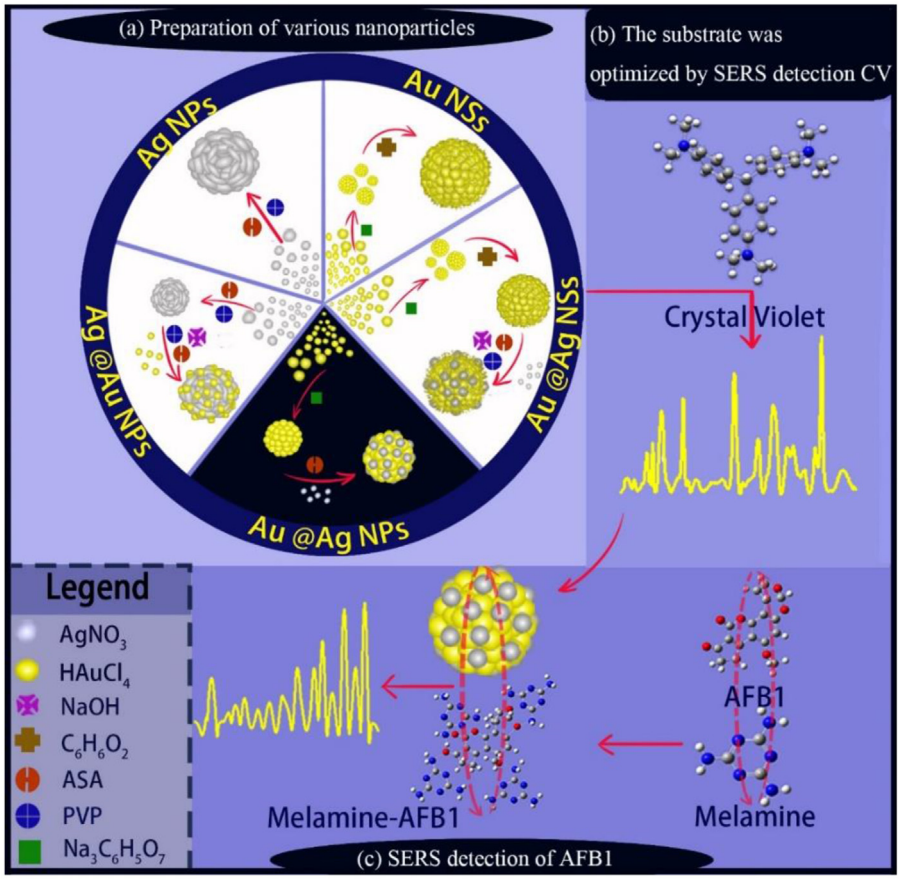

Fig. 1. Experimental flow chart. (a) Preparation of various nanoparticles. (b) The substrate was optimized by SERS detection CV. (c) SERS detection of AFB1.

different reactants in the control reaction system. The synthesis of Ag NPs is based on silver nitrate, which directly generates nanoparticles by adding reducing agents and surfactants. Then the small particles are polymerized to form flower-like aggregates. Au NSs were prepared by the seed-mediated method. Based on generating gold seeds, reducing particles of resorcin were added to make them agglomerate, and the star gold nanoparticles with long and sharp tips were easily grown. Au@Ag NSs are based on the highly agglomerated and rough morphology of Au NSs, then $AgNO_3$ is added to form the alloy. Ag@Au NPs take Ag NPs as the core and then adds $HAuCl_4$ to form the alloy. Au@Ag NPs are an alloy with silver particles wrapped in gold particles.

The characterization of different substrates was studied. Fig. 2 shows the SEM and TEM results of nanoparticles prepared under different growth conditions. Ag NPs and Ag@Au NPs have more surface bumps and fewer burrs. Au NSs and Au@Ag NSs had the largest particle size, but Au NSs had the most irregular burrs and the roughest surface. On the other hand, the particles of Au@Ag NPs are evenly distributed and dispersed, with an uneven surface, fewer burrs, and moderate roughness. Meanwhile, EDS-mapping results of the substrate are shown in Fig. 3. The uniformity of Au and Ag elements distribution can be observed, indicating that the structure of the nanoparticles is stable, and the sensitivity and stability are high.

In addition, the wavelength of SERS detection was selected according to the strongest absorption peak position of the substrate by referring to the UV–visible absorption spectrum shown in Fig. 4(a). As shown in Fig. 4(b), SERS spectral intensity from high to low was Au@Ag NPs, Ag NPs, Ag@Au NPs, Au NSs, and Au@Ag NSs. This is because of the morphology and material of the substrate. The particle size of Au@Ag NPs was small, and the sum of a specific surface area composed of multiple particles was the largest, so the SERS enhanced effect was the most obvious. According to the XRD pattern shown in Fig. 4(c), the prepared substrate

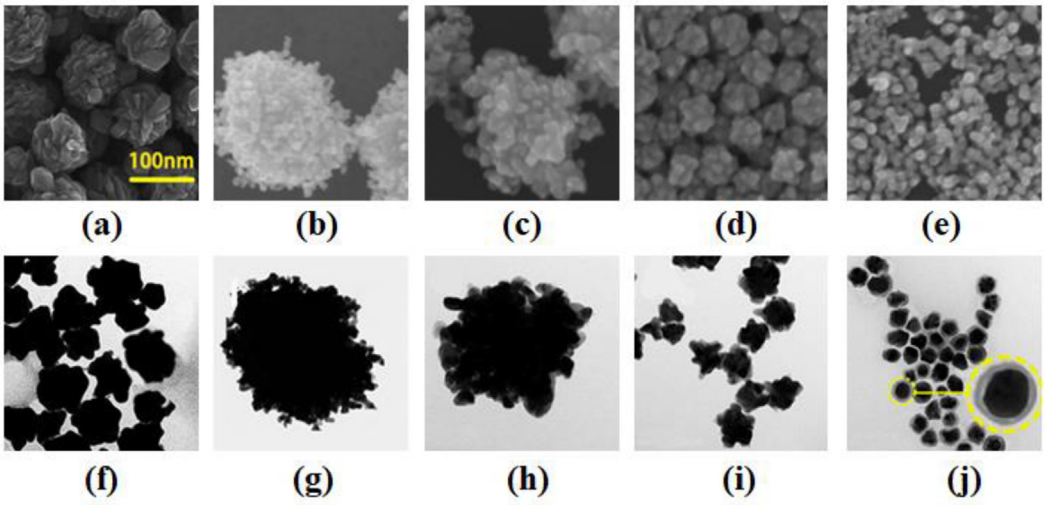

Fig. 2. SEM images of A series of nanoparticles:(a) Ag NPs. (b) Au NSs. (c) Au@Ag NSs. (d) Ag@Au NPs. (e) Au@Ag NPs. TEM images of a series of nanoparticles:(f) Ag NPs. (g) Au NSs. (h) Au@Ag NSs. (i) Ag@Au NPs. (j) Au@Ag NPs. Note: The scale in Fig. a applies to all the Figures. Fig. j shows the magnified morphology of nanoparticles.

has a polycrystalline structure, consisting of several small nanoparticles to form a large one. In Fig. 4(d), the core–shell structure of nanoparticles can be seen by FDTD.

According to the analysis of the above results, among the five kinds of nanoparticles, Au@Ag NPs have uniform morphology and a large sum of specific surface area with small particle sizes. It forms many coupling hot spots, which could increase the adsorption area and the number of molecules. It also creates a significantly enhanced electromagnetic field on its surface, resulting in its pronounced enhancement effect in SERS detection.

3.2. Sensitivity and repeatability detection of the substrate in the SERS spectrum

A crystal violet (CV) probe was used to detect the sensitivity and repeatability of the substrate, to evaluate whether the optimized Au@Ag NPs substrate can meet the detection needs. As shown in Fig. 5, typical Raman peaks of CV at 805 cm^{-1} (out of plane ring C–H bend), 920 cm^{-1} (skeletal ring vibration of radial orientation), 1187 cm^{-1} (in plane ring C–H bending), 1371 cm^{-1} (ring C–C stretching) and 1598 cm^{-1}, 1627 cm^{-1}(ring C–C stretching) can be observed [36]. It can be seen from Fig. 5(a) that when the concentration of CV is 10^{-9} M, the characteristic peak of the CV molecule still appears obviously, indicating that this substrate has high sensitivity. Besides, the SERS spectra of CV with 10^{-9} M and blank control were conducted and compared to investigate the background interference of the substrate prepared with Au@Ag NPs in the experiments. As Fig. 5(b) shows, we scarcely observe the substrate signals, which indicate the influence of a weak signal in the SERS detection.

The SERS mapping image of a substrate prepared with Au@Ag NPs demonstrated uniformity across the entire substrate to access spot-to-spot reproducibility. Each pixel at the spatial position symbolized the Raman intensity of CV at 1187 cm^{-1} (Fig. 5(c)). In addition, 20 points are selected randomly on the substrate for detection to investigate the substrate repeatability. The results are shown in Fig. 5(d), and the SERS spectra of CV with the same concentration show consistency. As shown in Fig. 5(e), the relative standard deviation (RSD) of peak strength at 920 cm^{-1} is 2.24%, and that at 1598 cm^{-1} is 2.21%, indicating that this method has high repeatability for SERS detection. As shown in Fig. 5(f), the relationship between the logarithm of the CV concentration and the intensity of the 1187 cm^{-1} peak is linear. The logarithm linear regression equation is $y = 9.36-7.32x$, and the linear correlation coefficient (R^2) is 0.9745. Thus, the result indicates that we could realize the quantitative detection of CV by measuring the change of SERS peak intensity.

In addition, a SERS substrate with good performance has a high SERS enhancement effect, and its long-term stability is an important performance index in practical applications. Fig. S1 (https://www.jfda-online.com/cgi/viewcontent.cgi?filename=0&article=3418&context=journal&type=additional) shows SERS spectra of crystal violet tested on the substrate under different storage conditions. It can

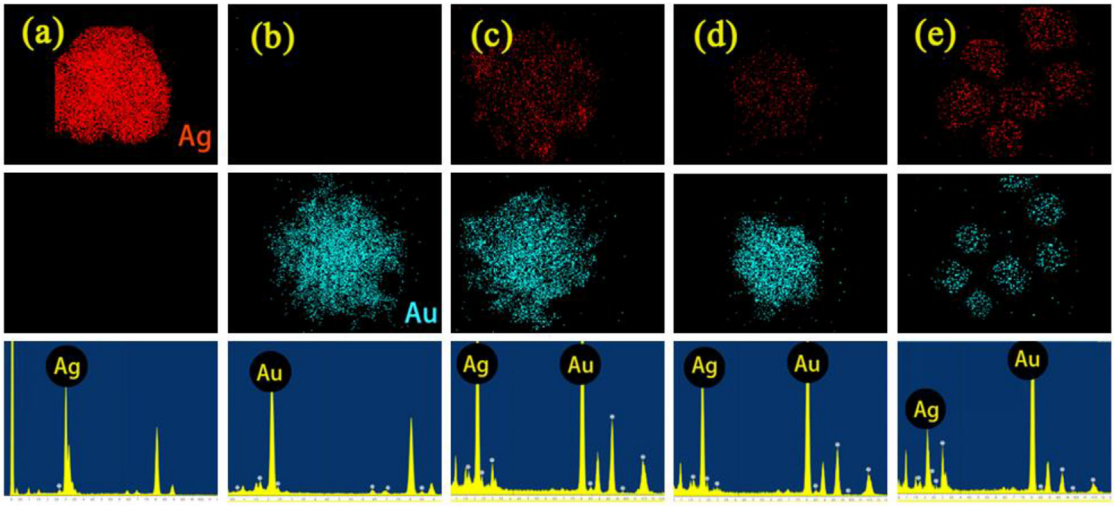

Fig. 3. EDS-Mapping of A series of nanoparticles:(a) Ag NPs. (b) Au NSs. (c) Au@Ag NSs. (d) Ag@Au NPs. (e) Au@Ag NPs. Note: The first row is the Ag element distribution, and the second row is the Au element distribution.

be seen that the SERS detection ability of substrates in the two storage environments decreases with time. However, after the substrate was stored in the refrigerator for 30 days, its spectral detection intensity was still significant, which was better than that of the substrate stored at room temperature.

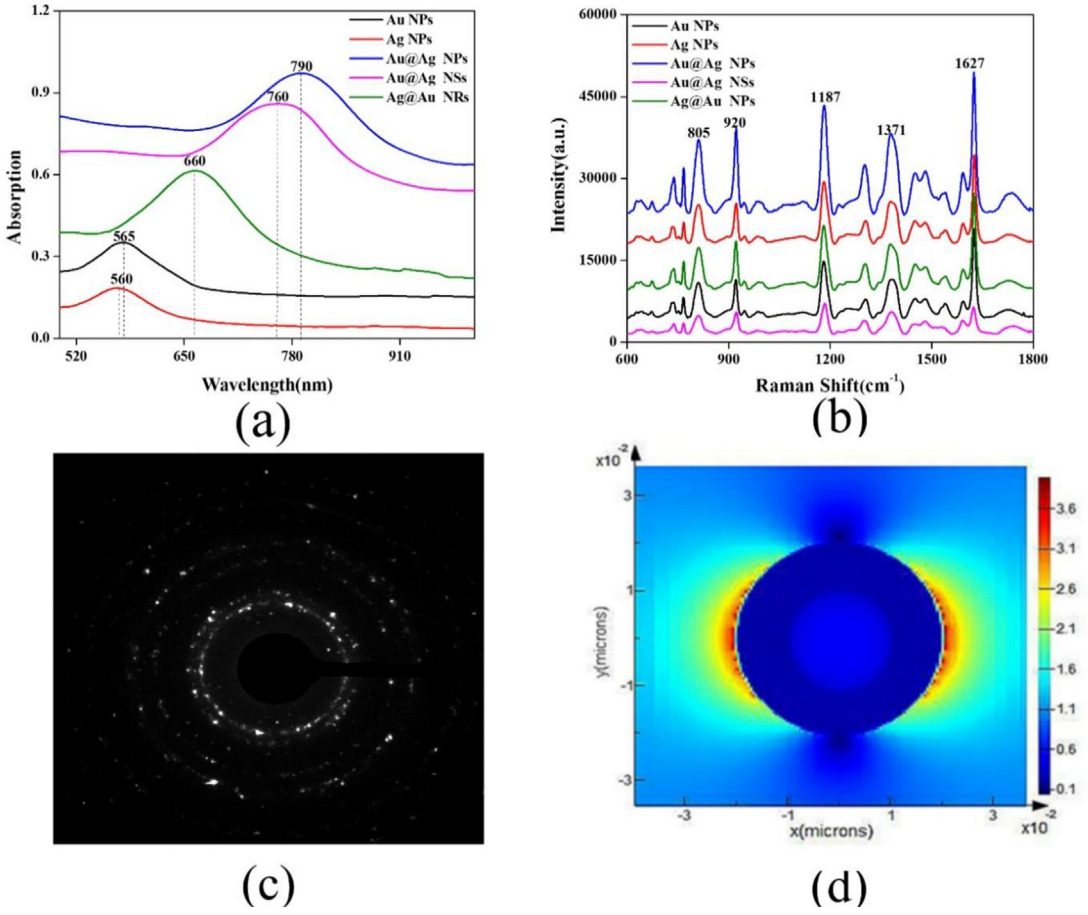

Fig. 4. (a) A series of UV–vis images of NPs. (b) SERS image of CV on a series of nanoparticle substrates. (c) XRD of Au@Ag NPs. (d) FDTD simulation of electric field distribution of Au@Ag NPs of different sizes in the x-y field of view.

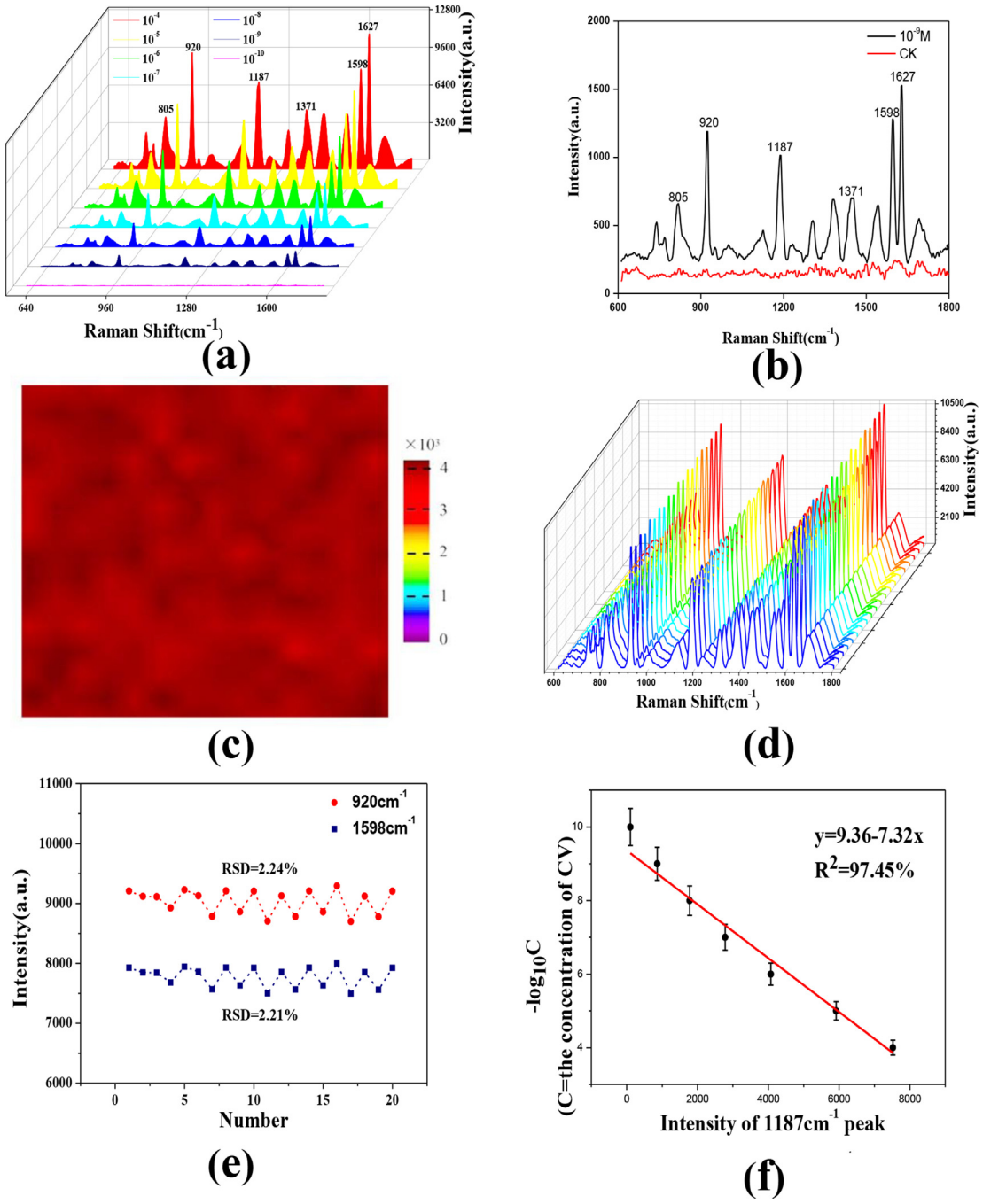

Fig. 5. (a) SERS spectra of CV with different concentrations on Au@Ag NPs substrate. (b) SERS spectra of CV (10^{-9} M) and blank substrate; (c) SERS mapping of CV (10^{-4} M) based on cactus-liked nanoparticles; (d) SERS spectrum of CV obtained from 20 random sites on Au@Ag NPs; (e) corresponding RSD values for peak intensity at 920 cm^{-1} and 1598 cm^{-1} for Au@Ag NPs. (f) the linear regression plot between Raman intensity of CV at 1187 cm^{-1} and the concentration of CV.

Therefore, under suitable storage conditions, the substrate has good stability.

3.3. SERS detection of AFB1

The above detection of CV probe molecules has determined that the Au@Ag NPs substrate has excellent sensitivity and repeatability to be further applied to detecting AFB1. However, because of the weak adsorption capacity between AFB1 and nanoparticles, the results obtained by conventional direct detection are poor when the substrate and AFB1 are mixed directly and dried for detection. Because AFB1 can interact with some compounds containing amino groups, an intermediate is used to bind with AFB1 and then mix it with the substrate for testing.

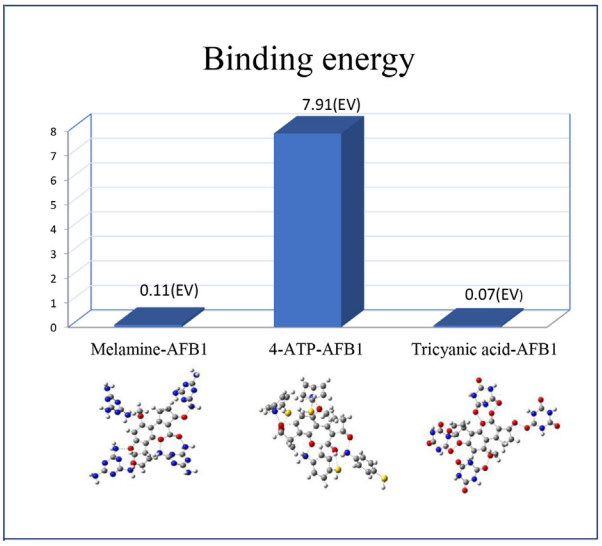

Fig. 6. The binding energy of melamine,4-ATP, Tricyanic acid, AFB1, and their compounds after optimization was calculated by DFT.

In selecting intermediates, melamine, 4-ATP, and tricyanic acid are compounds containing amino groups and have apparent characteristic peak positions in the SERS test when combined with the substrate, so they are selected for the next experiment. According to the DFT calculations [37,38] in Fig. 6, the binding energies of AFB1-melamine, AFB1-4-ATP, and AFB1- tricyanic acid are 0.11, 7.91, and 0.07, respectively. Therefore, melamine and 4-ATP are selected to combine with AFB1, respectively, for the subsequent SERS detection. As shown in Fig. 7(a), due to the strong binding ability of 4-ATP to the substrate, the apparent characteristic peak positions in the AFB1-4-ATP-Au@Ag NPs system are generated by 4-ATP, which is of little significance for the detection of AFB1. However, since the typical peak of melamine is only at 747 cm^{-1}, the characteristic peaks of melamine and AFB1 do not coincide, and the SERS detection of

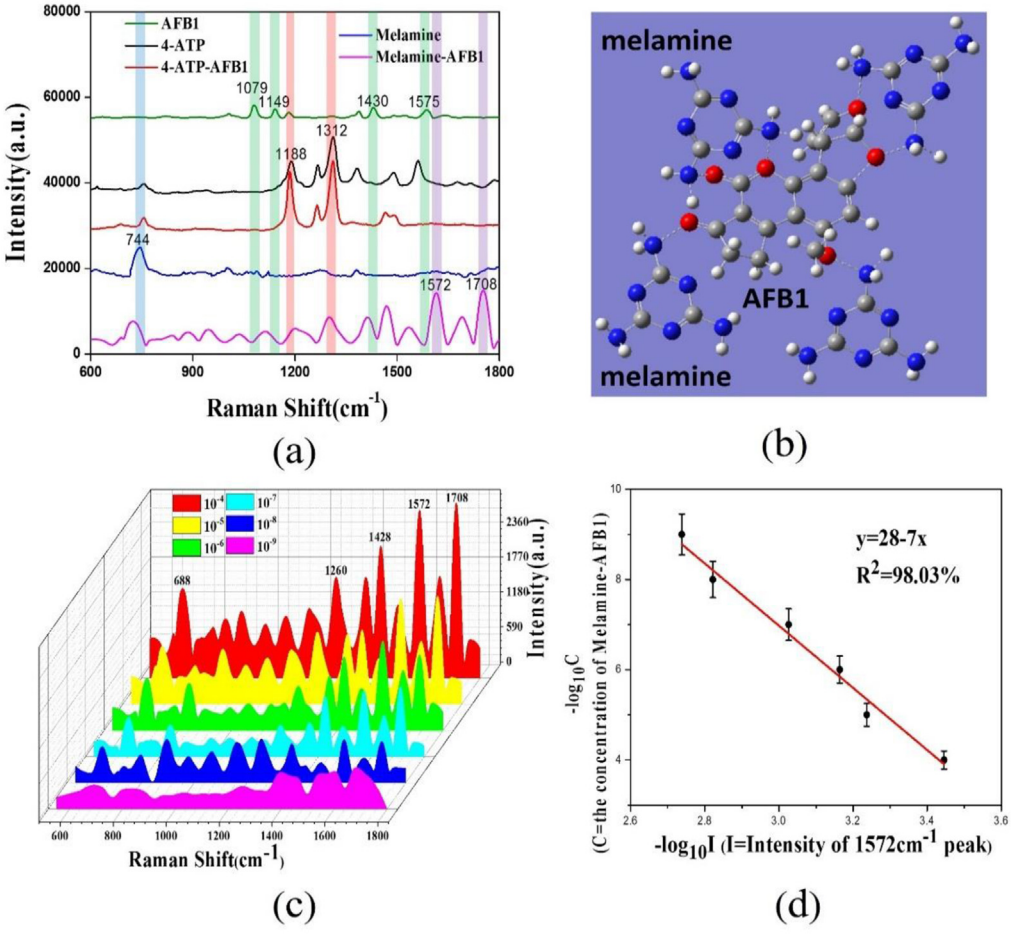

Fig. 7. (a) SERS spectra of 4ATP, melamine, AFB1 and their compounds on Au@Ag NPs substrate. (b) The optimized structure of AFB1-melamine complex obtained by DFT.(c) SERS spectra of AFB1-melamine complex with different concentrations on Au@Ag NPs substrate. (d) The Regression curve of AFB1-melamine complex.

AFB1 could be carried out effectively in the AFB1-melamine-Au@Ag NPs system.

Figure 7(b) shows the combination of melamine and AFB1. Hydrogen bonding force was formed between melamine and AFB1, conducive to SERS detection of AFB1 molecules. Subsequently, as shown in Fig. S2 (https://www.jfda-online.com/cgi/viewcontent.cgi?filename=0&article=3418&context=journal&type=additional), the optimal melamine concentration is further determined. The characteristic peak is the most significant at 10^{-5} M. At the concentration of 10^{-4} M, and melamine is adsorbed on at first, resulting in agglomeration of gold nanoparticles. However, melamine does not form hydrogen bonds with AFB1, resulting in a small amount of melamine trapped by hydrogen bonds. Therefore, the melamine characteristics summit masked the characteristic peaks of AFB1. On the contrary, if the concentration of melamine is too tiny, the hydrogen bond between melamine and AFB1 will be less, and the bond between melamine and gold nano will be weak, resulting in a weak detection signal.

Then, the gradient test of different concentrations of AFB1 is carried out. Figure 7(c) shows the SERS spectra of AFB1-melamine in concentrations varying from 1×10^{-4} M to 1×10^{-9} M and reveals characteristic peaks at 688 cm^{-1}, 840 cm^{-1}, 1260 cm^{-1}, 1428 cm^{-1}, 1572 cm^{-1} and 1708 cm^{-1}. Among them, 688 cm^{-1} is the vibration peak of the six-membered ring structure, 840 cm^{-1} is the vibration of the epoxy ring, 1260 cm^{-1} is the stretching vibration of the serial structure, 1428 cm^{-1} is the vibration of -och 2 - structure in the oxacyclic ring, both 1572 cm^{-1}, and 1708 cm^{-1} are C=C double bond vibrations in benzene derivatives. The above characteristic peaks can be judged as structural characteristics of AFB1. The results show that the detection limit is as low as 1×10^{-8} M, proving that the substrate has good SERS performance. For further evaluation, a quantitative analysis of AFB1-

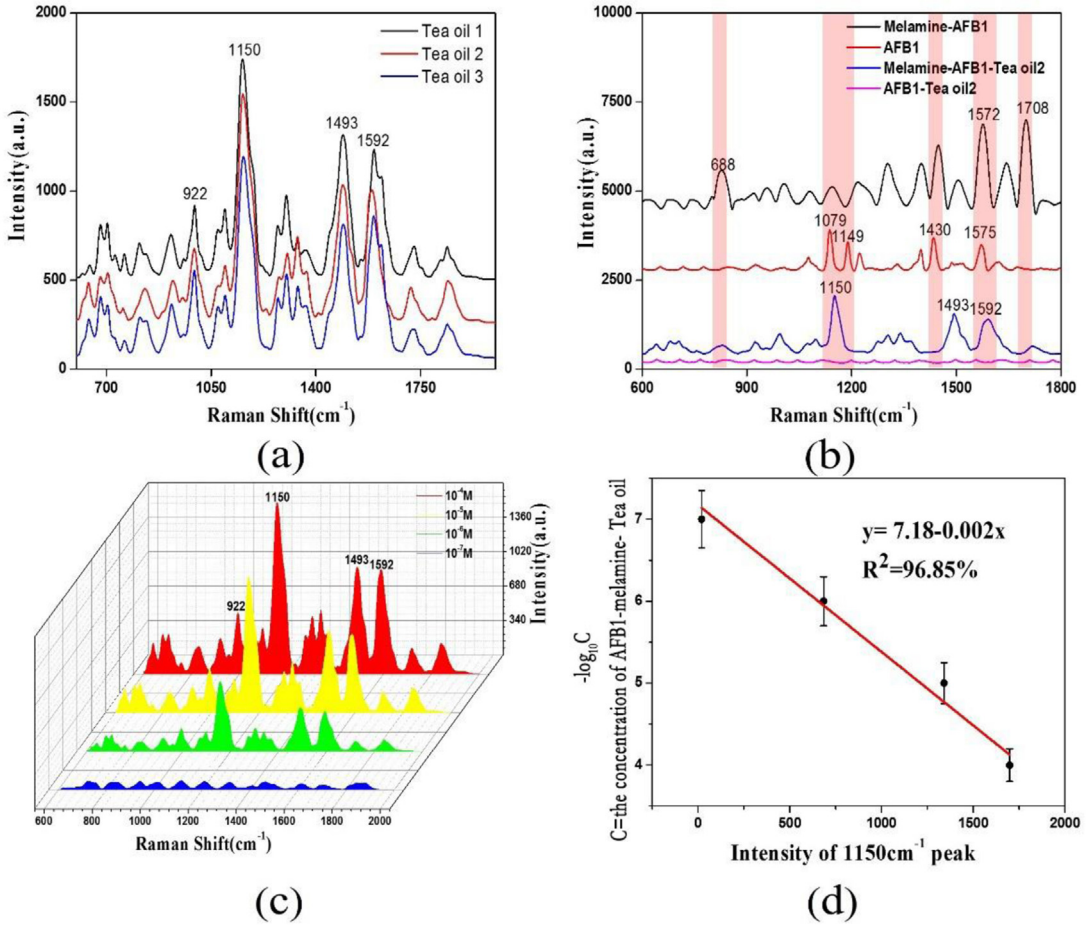

Fig. 8. (a) SERS detection of AFB1 with a uniform concentration in three different Tea oils. (b) SERS detection of various mixtures of melamine、, AFB1, and Tea oil. (c) SERS spectra of different concentrations of AFB1 in tea oil. (d) The Regression curve of AFB1-melamine- Tea oil complex.

melamine is conducted based on the characteristic peak of 1572 cm^{-1}. As shown in Fig. 7(d), the relationship between the negative logarithm of the AFB1-melamine and the peak intensity is linear. The logarithm linear regression equation is y = 28−7x, and the linear correlation coefficient (R^2) is 0.9803. The results indicate that we could realize the quantitative detection of AFB1 by measuring the change of SERS peak intensity.

We verified that the AFB1-melamine-Au@Ag NPs system could effectively detect SERS in AFB1 pure products through the above experiments. However, it is more meaningful to detect AFB1 in actual samples. Therefore, we selected three kinds of tea oil, mixed with AFB1 (10^{-4} M) respectively, and then detected by SERS. The experimental results are shown in Fig. 8 (a), and the three groups of data show similar maps. The specific performance is that the characteristic peaks are displayed at 922 cm^{-1}, 1150 cm^{-1}, 1493 cm^{-1}, and 1592 cm^{-1}. The peak intensity height is similar, which shows that this experimental method has good applicability in detecting the content of AFB1 in tea oil. Figure 8 (b) shows the results of SERS detection after combining several substances in the experiment. It further shows that the addition of melamine can more effectively adsorb AFB1 in tea oil on the substrate and achieve better SERS detection. Figure 8 (c) shows that we added different concentrations of AFB1 (10^{-4} M-10^{-7} M) to tea oil and then combined with melamine to detect the SERS spectrum on the substrate. The results showed that obvious characteristic peaks could be observed when tea oil contained AFB1 (concentration >10^{-7} M). Figure 8 (d) shows that the logarithmic linear regression equation between AFB1 and peak intensity is y = 7.18−0.002x. The linear correlation coefficient (R^2) is 0.9685, effectively detecting AFB1 of different concentrations in camellia oil. In addition, we compared a variety of SERS detection methods for AFB1 by referring to previous studies (Table S1 (https://www.jfda-online.com/cgi/viewcontent.cgi?filename=0&article=3418&context=journal&type=additional)). The previous detection mainly focused on SERS binding adapter technology, but the direct detection method in this study has great advantages.

4. Conclusion

Five kinds of nanoparticles were prepared under different growth conditions characterized by SEM, TEM, EDS-Mapping, XRD, FDTD, UV−Vis absorption spectrum, and SERS spectrum. The differences in morphology, size, and SERS enhanced effect among different nanoparticles were compared. Subsequently, CV was used as a probe molecule for the SERS test, and Au@Ag NPs were optimized as the best substrate. Then SERS detection of different concentrations of CV was carried out, proving that the substrate has high sensitivity and repeatability. The preparation of Au@Ag NPs is simple. The particles composed of small particles have a large sum of specific surface area, uniform morphology, high coupling hot spot, and obvious SERS enhanced effect. Then, the dosage of melamine was optimized, and the AFB1-melamine-Au@Ag NPs detection system was established. The minimum detection limit of AFB1 was 10^{-8} M, and the linear correlation coefficient was 0.9803. Therefore, in the study of AFB1, the AFB1-melamine-Au@Ag NPs system can be simple, convenient, and highly sensitive to realize the SERS detection of AFB1. Finally, we detected AFB1 in tea oil. The results show that when the concentration of AFB1 is more than 10^{-7} M, the linear correlation coefficient is 0.9685, which can be used for effective SERS detection. Hence, the prepared AFB1-melamine-Au@Ag NPs system provides the basis for detecting AFB1 and the promotion and application of SERS technology.

Funding

The work was financially supported by the National Key Research and Development Program of China (Grant No.2021YFD1000401), and the Hubei Provincial Water Resources Key Research Project (Grant No. HBSLKJT202001).

Conflict of interest

The authors declare no competing financial interest.

References

[1] Albero B, Sanchez-Brunete C, Miguel E, Tadeo JL. Application of matrix solid-phase dispersion followed by GC-MS/MS to the analysis of emerging contaminants in vegetables. Food Chem 2017;217:660–7.
[2] He H, Sun DW, Pu H, Huang L. Bridging Fe3O4@Au nanoflowers and Au@Ag nanospheres with aptamer for ultrasensitive SERS detection of aflatoxin B1. Food Chem 2020;324:126832.
[3] Ko J, Lee C, Choo J. Highly sensitive SERS-based immunoassay of aflatoxin B1 using silica-encapsulated hollow gold nanoparticles. J Hazard Mater 2015;285:11–7.
[4] Wang Q, Yang Q, Wu W. Progress on structured biosensors for monitoring aflatoxin B1 from biofilms: a review. Front Microbiol 2020;11:408 [In English].
[5] Jia Y, Zhou G, Liu P, Li Z, Yu B. Recent development of aptamer sensors for the quantification of aflatoxin B1. Appl Sci 2019;9 [In English].
[6] Caceres I, Khoury AA, Khoury RE, Lorber S, Oswald IP, Khoury AE, et al. Aflatoxin biosynthesis and genetic regulation: a review. Toxins 2020;vol. 12 [In English].

[7] Xue Z, Zhang Y, Yu W, Zhang J, Wang J, Wan F, et al. Recent advances in aflatoxin B1 detection based on nanotechnology and nanomaterials-A review. Anal Chim Acta 2019;1069: 1−27 [In English].
[8] Rushing BR, Selim MI. Aflatoxin B1: a review on metabolism, toxicity, occurrence in food, occupational exposure, and detoxification methods. Food Chem Toxicol 2019;124:81−100 [In English].
[9] Zhao Y, Yang Y, Luo Y, Yang X, Li M, Song Q. Double detection of mycotoxins based on SERS labels embedded Ag@Au core-shell nanoparticles. ACS Appl Mater Interfaces 2015;7:21780−6.
[10] Zhang W, Tang S, Jin Y, Yang C, He L, Wang J, et al. Multiplex SERS-based lateral flow immunosensor for the detection of major mycotoxins in maize utilizing dual Raman labels and triple test lines. J Hazard Mater 2020;393:122348.
[11] Wang X, Park SG, Ko J, Xiao X, Giannini V, Maier SA, et al. Sensitive and reproducible immunoassay of multiple mycotoxins using surface-enhanced Raman scattering mapping on 3D plasmonic nanopillar arrays. Small 2018;14:e1801623 [In English].
[12] Li J, Yan H, Tan X, Lu Z, Han H. Cauliflower-Inspired 3D SERS substrate for multiple mycotoxins detection. Anal Chem 2019;91:3885−92 [In English].
[13] Zhang CY, Zhao BC, Hao R, Wang Z, Hao YW, Zhao B, et al. Graphene oxide-highly anisotropic noble metal hybrid systems for intensified surface-enhanced Raman scattering and direct capture and sensitive discrimination in PCBs monitoring. J Hazard Mater 2020;385:121510.
[14] Perumal J, Wang Y, Attia ABE, Dinish US, Olivo M. Towards a point-of-care SERS sensor for biomedical and agri-food analysis applications: a review of recent advancements. Nanoscale 2021;13:553−80 [In English].
[15] Zhao Q, Liu G, Zhang H, Zhou F, Li Y, Cai W. SERS-based ultrasensitive detection of organophosphorus nerve agents via substrate's surface modification. J Hazard Mater 2017;324: 194−202.
[16] Fan M, Andrade GFS, Brolo AG. A review of recent advances in the applications of surface-enhanced Raman scattering in analytical chemistry. Anal Chim Acta 2020;1097:1−29 [In English].
[17] Liu G, Cai W, Kong L, Duan G, Li Y, Wang J, et al. Trace detection of cyanide-based on SERS effect of Ag nanoplate-built hollow microsphere arrays. J Hazard Mater 2013; 248−249:435−41.
[18] Xu Y, Kutsanedzie FYH, Hassan MM, Zhu J, Li H, Chen Q. Functionalized hollow Au@Ag nanoflower SERS matrix for pesticide sensing in food. Sensor Actuator B Chem 2020:324.
[19] Peralta-Videa JR, Zhao L, Lopez-Moreno ML, de la Rosa G, Hong J, Gardea-Torresdey JL. Nanomaterials and the environment: a review for the biennium 2008-2010. J Hazard Mater 2011;186:1−15.
[20] Lin S, Lin X, Han S, Zhao H, Hasi W, Wang L. Highly monodisperse Au@Ag nanospheres: synthesis by controlled etching route and size-dependent SERS performance of their superlattices. Nanotechnology 2019;30:215601.
[21] Bharadwaj S, Pandey A, Yagci B, Ozguz V, Qureshi A. Graphene nano-mesh-Ag-ZnO hybrid paper for sensitive SERS sensing and self-cleaning of organic pollutants. Chem Eng J 2018;336:445−55.
[22] Upadhyayula VK. Functionalized gold nanoparticle supported sensory mechanisms applied in the detection of chemical and biological threat agents: a review. Anal Chim Acta 2012;715:1−18.
[23] Xiaoyan Z, Ruiyi L, Xiaofei W, Zaijun L. A sensitive, switchable and biocompatible surface-enhanced Raman scattering-fluorescence dual-mode probe using bipyramid gold nanocrystal-gold nanoclusters for high-throughput biodetection. Anal Methods 2014;6.
[24] Yuan K, Zheng J, Yang D, Jurado Sanchez B, Liu X, Guo X, et al. Self-assembly of Au@Ag nanoparticles on mussel shell to form large-scale 3D supercrystals as natural SERS substrates for the detection of pathogenic bacteria. ACS Omega 2018;3:2855−64.
[25] Qu LL, Jia Q, Liu C, Wang W, Duan L, Yang G, et al. Thin layer chromatography combined with surface-enhanced Raman spectroscopy for rapid sensing aflatoxins. J Chromatogr 2018;1579:115−20 [In English].
[26] Yang M, Liu G, Mehedi HM, Ouyang Q, Chen Q. A universal SERS aptasensor based on DTNB labeled GNTs/Ag core-shell nanotriangle and CS-Fe3O4 magnetic-bead trace detection of Aflatoxin B1. Anal Chim Acta 2017;986:122−30 [In English].
[27] Nevels R, Welch GR, Cremer PS, Hemmer P, Phillips T, Scully S, et al. Figuration and detection of single molecules. Mol Phys 2012;110:1993−2000.
[28] Slag VM, Jung S, Rodriguez RS, Bourgeois M, Bryson S, Schatz GC, et al. Isothermal titration calorimetry for the screening of aflatoxin B1 surface-enhanced Raman scattering sensor affinity agents. Anal Chem 2018;90:13409−18 [In English].
[29] Wang J, Chen Q, Jin Y, Zhang X, He L, Zhang W, et al. Surface-enhanced Raman scattering-based lateral flow immunosensor for sensitive detection of aflatoxin M1 in urine. Anal Chim Acta 2020;1128:184−92 [In English].
[30] Wang W, Shu H, Wang J, Cheng Y, Liang P, Chen X. Defect passivation and photoluminescence enhancement of monolayer MoS2 crystals through sodium halide-assisted chemical vapor deposition growth. ACS Appl Mater Interfaces 2020;12:9563−71.
[31] An W, Yi -FH, Ujjal KS, De-YW, Bin R, Sandra R. In situ identification of intermediates of benzyl chloride reduction at a SilverElectrode by SERS coupled with DFT calculations. Chemical 2010;132:9534−6.
[32] Chen W, Li C, Yu Z, Song Y, Zhang X, Ni D, et al. Optimum synthesis of cactus-inspired SERS substrate with high roughness for paraquat detection. Spectrochim Acta Mol Biomol Spectrosc 2022;268:120703 [In English].
[33] Zhang D, Liang P, Yu Z, Huang J, Ni D, Shu H, et al. The effect of solvent environment toward optimization of SERS sensors for pesticides detection from chemical enhancement aspects. Sensor Actuator B Chem 2018;256:721−8 [In English].
[34] Asgari S, Sun L, Lin J, Weng Z, Wu G, Zhang Y, et al. Nanofibrillar cellulose/Au@Ag nanoparticle nanocomposite as a SERS substrate for detection of paraquat and thiram in lettuce. Microchim Acta 2020:187.
[35] Wang C, Wu X, Dong P, Chen J, Xiao R. Hotspots engineering by grafting Au@Ag core-shell nanoparticles on the Au film over slightly etched nanoparticles substrate for on-site paraquat sensing. Biosens Bioelectron 2016;86:944−50.
[36] Wei W, Huang Q. Preparation of the cellophane-based substrate and its SERS performance on the detection of CV and acetamiprid. Spectrochim Acta Mol Biomol Spectrosc 2018;193:8−13.
[37] Wu X, Gao S, Wang JS, Wang H, Huang YW, Zhao Y. The surface-enhanced Raman spectra of aflatoxins: spectral analysis, density functional theory calculation, detection, and differentiation. Analyst 2012;137:4226−34 [In English].
[38] Chen Q, Jiao T, Yang M, Li H, Ahmad W, Hassan MM, et al. Pre etched Ag nanocluster as SERS substrate for the rapid quantification of AFB1 in peanut oil via DFT coupled multivariate calibration. Spectrochim Acta Mol Biomol Spectrosc 2020;239:118411 [In English].